Evolution of surface roughness of single sand grains with normal loading

Ting Yao[1], Beatrice A. Baudet[2*], Sérgio D.N. Lourenço[3]

1. Sate Key Laboratory of Geomechanics and Geotechnical Engineering, Institute of Rock and Soil Mechanics, Chinese Academy of Sciences, Wuhan, P. R. China
2. Department of Civil, Environmental and Geomatic Engineering, University College London, London, U.K.
3. Department of Civil Engineering, The University of Hong Kong, Hong Kong, P. R. China

* Corresponding Author

Author lists:

Ting Yao[1], Sate Key Laboratory of Geomechanics and Geotechnical Engineering, Institute of Rock and Soil Mechanics, Chinese Academy of Sciences, Wuhan, P. R. China, yaoting98@163.com.

Beatrice A. Baudet[2*], Department of Civil, Environmental and Geomatic Engineering, University College London, London, U.K., *Corresponding author: b.baudet@ucl.ac.uk.

Sérgio D.N. Lourenço[3], Department of Civil Engineering, The University of Hong Kong, Hong Kong, P. R. China, lourenco@hku.hk.

Abstract

The surfaces of soil grains are not perfectly smooth especially examined at small scale. In geotechnical engineering, surface roughness has been found to be able to influence the inter-particle friction angle at micro scale and small-strain stiffness at macro scale. However, the quantity and quality of the studies on surface roughness of natural soils are still limited. In this study, the evolution of surface roughness of natural sand grains with increasing normal load was investigated by a single particle compression apparatus. Thirty Leighton Buzzard sand (LBS) grains coarser than 2.36 mm were tested, and the surface roughness was measured before and after compression by an optical interferometer. The deformations of the asperities and of the bulk of the sand grains in the vicinity of the contact were mapped. Three stages were identified as the normal load increased: (1) plastic deformation of the asperities, (2) asperities and bulk plastic deformation and, (3) bulk only plastic deformation. At very small normal load, only the asperities were found to deform plastically, and the surface roughness of the sand grains decreases due to the flattening of the asperities. Within this regime, the load-displacement relationship of LBS grains under compression could be simulated by the modified Hertz model which takes surface roughness into consideration. With increasing normal load, the bulk of the sand grains began to yield near the contact. The geometry of the surfaces of LBS grains in contact with the loading platen is the main factor that influences the plastic deformation of the bulk. Different from the plastic deformation of the asperities, the plastic deformation of the bulk could both smoothen and roughen the surfaces. When plastic deformation of the bulk occurred, both Hertz and modified Hertz theory could not predict the load and displacement relationship of sand grains. Through analysing the cumulative distributions of surface roughness of thirty LBS grains at different normal loads by the Weibull function, the surface roughness was found to decrease dramatically with increasing normal load at first and then tend to be constant.

KEYWORDS: single particle compression test; surface roughness; plastic deformation; load-displacement relationship

Introduction

Natural soil grains vary in shape and surface texture, which both can influence the behaviour at the micro- and macro-scale. The surface roughness affects the inter-particle friction coefficient (e.g. Senetakis *et al*., 2013; Nardelli & Coop, 2019; Sandeep & Senetakis, 2018a) and contact behaviour (Cavarretta *et al*., 2010; Cavarretta *et al*., 2012), effect which has been found to attenuate with increasing stress level, eventually reverting to being Hertzian (i.e. typical of smooth surfaces) at pressures well in excess of those typically encountered in a soil sample. Soil grains' surface roughness also influences element scale behaviour, e.g. the small strain modulus (e.g. Santamarina & Cascante, 1998; Yimisiri & Soga, 2000; Otsubo *et al*., 2015), up to medium to high stresses. For the majority of simulations performed by the discrete element method (DEM), the contact law does not take account of the grain's roughness. As more realistic contact models for DEM are needed, so are experimental data, but they have so far been limited (Cavarretta *et al*., 2010; Nardelli, 2017; Nardelli *et al*., 2017; Sandeep & Senetakis, 2018b; Nardelli & Coop, 2019).

The effect of surface roughness on contact mechanics is not specific to soils, and a vast amount of work exists for application to engineered materials or thermo-conductors (e.g. Cooper *et al*., 1969; Greenwood & Tripp, 1967; Greenwood *et al*., 1984; Kogut & Etsion, 2003). Models that have been proposed for rough contacts tend to be purely theoretical, based on the assumption that asperities deform, with a constant value of roughness during loading despite the large number of experimental results demonstrating that the surface roughness of both engineered materials (e.g. Hanaor *et al*., 2013 on aluminium rods; Cavarretta *et al*., 2010 on glass ballotini) and natural soil grains (e.g. Altuhafi & Coop, 2011; Nardelli & Coop, 2019) is susceptible to change, under compression or shearing, at inter-particle level or within a soil element. Adopting a constant roughness parameter is also not consistent with the model assumption that asperities deform. A systematic investigation of the change of surface roughness of real soil grains under loading could contribute to a deeper understanding of their contact mechanics.

Hertz' (1882) theory of contact between two smooth spherical solids is widely used: a contact area is formed when the two spheres are pressed against each other, which depends on the load and particle geometry and elastic properties. A summary of the essential equations is given in Appendix A. For most surfaces, which are not ideally smooth, contacts occur first at the asperities. There have been different approaches to modelling the contact between rough surfaces: a popular approach is to assume that the asperities deform elastically following Hertz (e.g. Greenwood & Tripp, 1967; Yimsiri & Soga, 2000), but more recently the importance of plasticity in rough contact mechanics has been recognised (e.g. Greenwood & Wu, 2001; Bahrami *et al*., 2004) while more advanced elastoplastic models have also been proposed (e.g. Chang *et al*., 1987; Persson, 2001; Li et al., 2010). The modified Hertz' model (Appendix B) includes effects of roughness in the size of the contact area between two rough spheres, which is then implemented into Hertz' model. It is implicitly assumed that asperities and bulk deform elastically, although others have argued that while overall stresses may be small and within the elastic region of the material, stresses at the asperities are higher and plastic yield may occur (Holm, 1938). In Hertz' theory, where deformations are assumed to be purely elastic, the area of contact is a power function of the load, typically with an exponent equal to 2/3, thus Amonton's friction law is not satisfied. If asperities deform plastically, the total area of contact will increase proportionally to the load and the friction law will be satisfied. Archard (1957) demonstrated that even when elastic behaviour is observed, the load power exponent tends to unity (i.e. the friction law applies) if the contacting surfaces touch at an increasing number of small areas. One of the key factors is therefore whether an increase in load creates new contacts, which supports the hypothesis of a fractal surface or whether it increases the size of the existing contact areas, which deform with the effect of reducing the roughness. Recent elastic-plastic models for contact behaviour address the proportionality between displacement and load by assuming that the load exponent varies between 0.66 (2/3) and 0.80 depending on a critical load depending on the yield strength and the geometrical and elastic properties of the solid bodies (Li et al., 2010). In tangential loading, Weber *et al*. (2018) have shown that at the contact between polystyrene or glass spheres and a smooth flat surface, there are both elastic interaction between asperities and contact plasticity of the asperities. In soil mechanics, there is no experimental evidence that could help channel the effort in modelling the mechanics at particle contact. A possible change in roughness with loading is also neglected.

In this paper, we present the evolution of surface roughness of natural sand grains when subjected to one-dimensional compression. Tests were carried out on a quarzitic sand using a custom-made single particle compression apparatus. The surface roughness of the grains was determined before and after compression by optical interferometry, and the deformations of the asperities and of the bulk of the grains were assessed. The applicability of using Hertz' theory and modified Hertz' theory, which takes account of surface roughness, both widely used in DEM to predict the load-displacement of the sand grains, is discussed.

Experiments

Materials

Leighton Buzzard sand (LBS), a quarzitic sand found in the UK, was tested. With relatively spherical and rounded shape as shown in Fig. 1(a), it was chosen because of its good reflectivity which allows for satisfactory surface roughness measurement by optical interferometry (e.g. Yang *et al*., 2016; Yao *et al*., 2018). The non-flat shape and generally poor reflectivity of natural sand grains makes measuring their roughness difficult, in particular by interferometry, and in previous work roughness is usually estimated from single-point-on-single-grain data, and/or from a limited amount of grains. In order to obtain a statistical representative result, here thirty LBS grains of size 2.36-5 mm were tested, a number typically used in studies on single particles, such as to determine particle characteristic strength (e.g. Cavarretta *et al*., 2017), and it was found by Yao (2019) to give stable characteristics roughness values from statistical analyses. Sand grains with only one apex in its most stable position were used to simplify the identification of the spot being compressed. The diameter of each grain was measured by an electrical calliper at three principle directions. Table 1 summarizes the mean values of the diameters of the tested grains and the mechanical properties of LBS including Young's modulus (E), shear modulus (G), Poisson's ratio (v), and micro-hardness (H) (Mavko *et al*., 1998; Jaeger *et al*., 2007; Wang, 2017). All the grains were cleaned by tap water and then oven dried. Prior to the measurement of surface roughness, they were cleaned again by alcohol to remove any surface contamination.

Apparatus

A custom-made single particle loading apparatus was designed to investigate the change of surface roughness of sand grains under uniaxial compression. A schematic diagram of the apparatus is shown in Fig. 1(b). A hardened stainless-steel flat loading platen (H=7.5 GPa, E=210 GPa and v=0.3), of 10 mm diameter, was used to compress the individual grains. The vertical movement of the platen, entrained by a micro-step motor (NA14B30-T4-MC04, Zaber Technologies Inc.), applied a normal load measured by a load cell (F245CF00H0, NovaTech) of resolution of 0.5 N and capacity of 400 N. The deformation of the sand grains was measured by a linear variable differential transformer (LVDT) (D6/02500U-L50, RDP Electronics Ltd.) with a finite resolution of 0.5 μm, its armature screwed on the lower platen to minimize the effect of its movement on the accuracy of displacement. A computer written program in QBASIC (personal communication with Professor Matthew Coop) enabled both displacement- and load-controlled tests.

The surface roughness was measured using an optical interferometer (Fogale, 2005) with a horizontal resolution of 0.184 μm, a vertical resolution of around 10 nm, and a maximum size of field of view of 107×140 μm^2. Based on the findings of Yao *et al*. (2018) for LBS grains, the size of field of view of 106.6×106.6 μm^2 was used to minimize the occurrence of invalid pixels which could influence the reliability of roughness. This also maximised the possibility that the contact area between the sand grains and the loading platen be within the size of field of view: using the properties of the platen and of the grains (Table 1), Hertz' theory would predict a contact radius between 66 and 146 μm for loads of 10 to 100 N. The surface roughness was quantified by the flattened root-mean-square roughness (RMS_f) of the raw height data from the mean plane obtained after separating the roughness from the shape of the surface by the motif extraction method (Boulanger, 1992). This measurement is embedded into the interferometer software, FOGALE Pilot 3D software for data capture and FOGALE Viewer 3D software for data analysis. When the size of field of view is 106.6×106.6 μm^2, the numbers of points along two directions are both 578 and the shape motif used to flatten the surfaces is 26.6 μm. The surface roughness of the loading platen was measured at 8 points at the central part, which is most likely to be in contact with the sand grain during loading: a mean value of RMS_f = 0.198 μm was determined. The limitation of this method, which uses different scales to fit the shape of sand grains of different sizes (e.g. Otsubo *et al*., 2014; Yang *et al*., 2016), was minimised by using sand grains of similar size and apparent shape. The grain-to-hard platen setup allowed carrying out a number of tests significant enough to be statistically reliable, as well as allowing checking the roughness evolution at a given point of the sand grain, and although particle-to-particle tests as those carried out by Nardelli & Coop (2019) would be more representative, they are difficult to implement and rarely performed in large numbers.

Testing procedures

The LBS grains were glued to a purposely-made stainless-steel holder by super glue (Araldite) at least 48 hours prior to being compressed to avoid any rotation of the grain during test. After creating a small circular pit of 4 mm diameter and 0.3 mm depth on top of the holder, a drop of super glue was put into it then a sand grain was placed there along its most stable direction and pressed slightly against the holder with the tweezers to let the glue underneath flow towards the external sides of the grain and minimize the thickness of the glue at the bottom.

After 48 hours, the sample (grain in its holder) was placed onto the platform of the interferometer to measure the surface roughness at the apex of the grain, which is most likely to be in contact with the loading platen. The sample was then moved to the single particle compression apparatus and the holder was screwed tightly to the base of the apparatus (see Fig. 1b). The loading platen was moved downwards, controlled by the linear actuator and the grain was subsequently compressed to the designed load level with a displacement rate of 0.2 mm/h. The loading series was 1 N, 2 N, 4 N, 10 N, 20 N, 40 N, 60 N, 80 N, 100 N, 120 N and 150 N (maximum value estimated from the single sand particle strength), or until the grains crushed. Note that limited data for granular assemblies, based on DEM simulations (e.g. Barreto Gonzalez, 2009) or a combination of X-ray computed tomography and micro-finite element analysis (Nadimi et al., 2020) report inter-particle forces between 3 and 6 N at confining pressures of 100 kPa, which suggests that forces between 40 N and 150 N represent stress levels between 1 MPa and 3 MPa, found in pile end bearing or underneath high earth dams. Restricted by the resolution of the load cell, the minimal normal load during tests was around 1 N. After the grain was loaded to the required value, the load was held for 3s for system stabilization and then it was unloaded with a displacement rate of 0.2 mm/h.

After each compression stage, the sample was placed back on the platform of the optical interferometer to measure the surface roughness at the same point. The similarity of the surfaces has been carefully assessed to guarantee the consistency of the measurement points before and after compression. Grains that did break under load were excluded from these measurements, so measurements were limited to pre-failure. The change in roughness was quantified using the ratio proposed by Altuhafi & Coop (2011):

$$Ratio = \frac{RMS_{fn} - RMS_{fi}}{RMS_{fi}} \times 100 \quad (1)$$

where RMS_{fn} is the root-mean-square surface roughness of the tested sand grain after the *n*th compression stage, and RMS_{fi} is the initial surface roughness of the LBS grain.

Yao (2019) showed that Weibull's cumulative distribution function (CDF, 1951) represents well the cumulative distributions of sand grains surface roughness in their natural state (i.e. not under loading):

$$CDF = 1 - e^{-(x/\lambda)^k} \quad (2)$$

where CDF is the cumulative distribution percentage of variable x, λ is the scale parameter, $k>0$ is the shape parameter of the distribution. The cumulative distributions of surface roughness of the thirty LBS grains measured at the different normal loads were fitted by the Weibull CDF to obtain a representative value of the roughness and of its variability. A value of λ corresponding to (1-1/e) can represent the surface roughness (note that it is different from the survival probability usually applied to soil grain strength, which corresponds to 1-CDF). The parameter k describes the wideness of the surface roughness distribution, which value increases with decreasing variability in surface roughness of the grains.

Compression may induce plastic deformation of the asperities but also of the bulk, and as these would remain after unloading, they can be assessed from the images obtained at different stages of loading. It is difficult in practice to identify the plastic deformation of sand grains from the three-dimensional images obtained by optical interferometry, so here it was determined from 2D profiles of the surfaces, following Jamari & Schipper (2007) who quantified the plastic deformation of a flat deformable aluminium surface caused by indentation based on optical interferometer data. The profiles of the horizontal lines along the X direction at the centre of the Y direction of the surfaces were used, as it is hypothesized that the centre of the sand grains experiences the largest plastic deformation under compression.

Results and discussion

Plastic deformation of the asperities and the bulk

From the tests on thirty LBS grains, three main types of contact behaviour were detected: the majority of grains mainly experienced plastic deformation of the asperities, but four grains failed during compression after experiencing plastic deformation and two grains experienced plastic deformation of the bulk without failure. The behaviours of three selected grains, LBS2, LBS5 and LBS26, each representing one type of these deformation patterns, are presented and discussed below. Statistical results for the whole 30-grain sample are presented later.

Results for grain LBS5 are presented in Figs 2 to 5(a). LBS5 developed cracks and failed before reaching the maximum load of 150 N. The three-dimensional images of the grain surface in contact with the loading platen before and after compression to 1 N (Fig. 2) show a high degree of similarity, illustrating the high consistency of the surfaces measured before and after compression, and thus demonstrating the reliability in detecting and quantifying surface roughness changes. The asperities at the central part of the surface were flattened under compression, over a contact area smaller than the size of field of view, indicating that plastic deformation of the asperities can occur even at a relatively low load. This was corroborated by a decrease in measured surface roughness RMS_f from 0.393 μm before test to 0.369 μm after loading to 1 N. The two-dimensional profiles along the X direction, at the position of Y=53.3 μm, before and after loading, are presented in Fig. 3. The curvature of the profile and the asperities at the surroundings were not deformed, suggesting that if deformation of the bulk occurred, it was elastic. It is inferred that for that grain, contact between the particle and the loading platen occurred first at the asperities, over a small contact area, so that the pressure at the contact was initially high despite the low load, beyond the hardness of the asperities which then deformed plastically.

Subsequent loading stages were applied, with the surface roughness measured after each compression. Because of the occurrence of cracks, which is linked to the strength and geometry of the grain, the test was stopped at the load of 80 N. The evolution of the surface with increasing normal load, presented as three-dimensional images in Fig. 4, shows that the plastic contact area between the grain and the rigid loading platen increases with increasing normal load, exceeding the size of field of view for surface roughness measurement at the load of 80 N. The profiles of the centre line along the X direction of the surfaces at different load levels are combined in Fig. 5(a). At loads smaller than 40 N, plastic deformation only occurred at the asperities, the number and contact area of the asperities increasing with normal load. The deformation reached a magnitude of 0.5 μm at 40 N, while very little change occurred in the curvature of the profile. Small cracks appeared on the surface at 60 N, resulting in the flattening of the curvature, that is bulk plastic deformation. At that stage, the plastic deformation of the bulk in the vicinity of the contact dominated the deformation behaviour as the plastic deformation of the asperities (0.5 μm) was much less than that of the bulk (2.5 μm). Examination of all the grains that failed before reaching the load of 150 N revealed that for LBS sand grains the failure is usually accompanied by significant plastic deformation and alteration of the surface roughness.

Another selected grain, LBS2, suffered significant plastic deformation although cracks did not happen. Figure 5b presents the profiles of the surface of LBS2 (initial RMS_f=0.439 μm) with increasing normal load. For loads below 20 N, plastic deformation only occurred at the asperities. Marked bulk deformation was observed near the contact at the load of 40 N, which is indicated by the different datum of the profiles. For loads above 40 N, the deformation behaviour was dominated by the plastic deformation of the bulk, which increased with increasing normal load. This demonstrates that significant plastic deformation for LBS grains is not solely caused by particle breakage. The plastic contact area between LBS2 and the loading platen was always within the size of field of view (106.6×106.6 μm^2).

The majority of the sand grains mainly experienced deformation of the asperities, even at very high loads, or sometimes a combination of asperities with small bulk plastic deformation near the contact. The profiles of LBS26 (initial RMS_f=0.329 μm) at each compression stage are shown in Fig. 5(c) as a typical example. Only a limited number of asperities underwent plastic deformation, while the curvature of the profile was not deformed until the load reached 80 N. The plastic deformation of LBS26 remained lower than those observed for LBS5 and LBS2, even at 150 N.

Based on the results presented above, the contact behaviour of LBS grains under normal load against a hard platen could be described in three stages: (1) The contact between the two rough surfaces occurs first at the asperities, with plastic deformation occurring in some asperities while the deformation of the bulk is elastic. (2) With increasing load, the number of asperities subjected to plastic deformation increases, and the possibility for the bulk to yield near the contact increases. The plastic deformation of the asperities is comparable to that of the bulk when it yields, suggesting elasto-plastic behaviour, where the plastic deformation comprises that of both the asperities and the bulk. (3) The bulk plastic deformation develops until it dominates the plastic deformation of the particle, so the contact response could be described as elastic bulk-plastic.

Effect of the local surface curvature on the plastic deformation

Theoretically, yield of the bulk occurs when the maximum Hertz pressure is higher than a threshold value associated with the hardness of the solids under compression (Tabor, 1951). In our experiments, although care was taken to test grains of similar shape, grains yielded at different loads, and exhibited different contact responses. It was shown by Zhao *et al*. (2015) and Wang & Coop (2016) that the real contact area between sand grains and loading platen is more related to the shape of the corners in contact rather than the global shape of the sand grain. The commonly used roundness factor first proposed by Wadell (1932) to describe the sharpness of the corners of a grain is scale dependent and ignores surface concavities which, in the case of natural sands, may occur due to their irregular shape. A recent study by Brzesowsky *et al*. (2011) showed the effect of an equivalent radius of curvature on the critical force of grains at failure, defined as the product of the square roots of the maximum and minimum radii of curvature. Wang & Coop (2016) defined a local roundness parameter which is the ratio between the radii of curvature of the contact surface and of the maximum inscribed circle of the grain outline. Here, we use an average radius of curvature derived from the radii of curvatures of the grain contacting surface, R_x and R_y, in the X and Y directions:

$$R_c = \sqrt{R_x^2 + R_y^2} \tag{3}$$

Figure 6 illustrates how to calculate R_c from the profiles of the centre lines of the surface in the X and Y directions captured by the optical interferometer, where the radius of the curvature in the X or Y direction was estimated by the following equation (using R_x as an example):

$$R_x = \frac{h_x^2 + l_x^2}{2h_x} \tag{4}$$

where l_x is the half-length of the projection in the X direction and h_x is the height of the profile as shown in Fig. 6(b).

In Fig. 7, the normal load at which bulk plastic deformation occurred is plotted against the curvature of the contact surface ($1/R_c$) with the view to understand the influence of the curvature at the contact on the development of bulk plastic deformation. Bulk plastic deformation was observed in the vicinity of the contact in the thirty LBS grains at normal loads higher than 40 N. The more angular grains, with higher local surface curvature, tended to yield earlier than those with more rounded corners. This is because of higher effective central pressure, and also because when the contact is concentrated on a smaller surface, the asperities tend not to behave independently.

The plastic deformation of the sand grains therefore not only increases with normal load, but it is also affected by the curvature of the surface in contact with the loading platen. Figure 8 shows an example of the quantification of the plastic deformation using the profiles of the centre line of the contact surface in the X direction for a certain loading stage. From Fig. 9(a), showing data for particles under a normal load of 60 N, the combined plastic deformation of the asperities and bulk shows a positive trend with the surface curvature. The same trend, i.e. higher surface curvatures lead to larger plastic deformation, is found for the higher load of 150 N (Fig. 9b).

Applicability of Hertz models to the load-displacement relationship

Although it has been demonstrated on engineered materials that the hypothesis of elastic or plastic deformation at the contact does not affect the predictions significantly, this has not been shown for sand grains, and since elastic contact theories such as Hertz' or modified Hertz' model are widely used to model the contact behaviour of sand grains, the experimental results here highlight a need for discussing their applicability.

Figure 10(a) shows a comparison between the experimental result obtained for LBS5 loaded at 1 N and the predictions from classical and modified Hertz theory using the properties in Table 1 for the sand grains, and the RMS_f^* quoted in the figure which is the combined roughness of the sand grain and the loading platen (RMS_f=0.325 μm) for the modified Hertz model. The softer response obtained experimentally cannot be predicted, although as was observed by Nardelli & Coop (2019), the modified model, which takes account of roughness with the parameter α, described the trend of the curve better, especially at low displacements. The differences are attributed to the permanent deformation of the asperities, and they are more significant at a higher load of 40 N, as shown in Fig. 10(b), where it is thought that the flattening of the asperities under loading caused an increase in stiffness of the particle.

For grain LBS2, which developed plastic bulk deformation near the contact after 40 N (see Fig. 5b), the gap between experimental and predicted data increased with normal loading, as seen in Figs 10(c) and 10(d) for normal loads of 40 N and 150 N. Note that for most models including Hertz', bulk deformation is assumed to occur only in the vicinity of the contact, with no deformation assumed far from the contact, and in this study bulk deformation was measured in the vicinity of the contact.

A similar comparison is shown for grain LBS26 at the loads of 40 N (Fig. 10e) and 150 N (Fig. 10f). From Fig. 5(c), the deformation of this particle is mainly elastic until the final compression stage of 150 N. It is therefore expected that the difference between the experimental data and the prediction by the modified Hertz theory at the load of 40 N should be insignificant. The sudden decrease of the stiffness of the particle at 100 N, observed from the displacement curve in Fig. 10(f), might be caused by a late onset of bulk plastic deformation. Overall, the deformation of the asperities is negligible compared to the elastic bulk deformation so that the contact behaviour can be successfully simulated by the modified Hertz model. Once the plastic deformation of the bulk occurred, the relationship between load and displacement could not be modelled by the elastic contact theory anymore.

Analysis of surface roughness evolution on single grain and for grain sample with a statistical function

Flattening of the asperities occurred from the initial contact between the grain surfaces and the rigid platen (Figs 2-4). With increasing normal load, the plastic contact area increased gradually, likely due to a combination of more contact points being created and the contact area increasing under pressure. This flattening of the asperities can result in a change in the surface roughness, as was mentioned above for 1 N normal load. The surface roughness of the three selected LBS grains (LBS2, LBS5 and LBS26) was measured at each stage of increasing normal load to gain insight into what affects the change in roughness more, the plastic deformations of the asperities, of the bulk or both.

Figure 11(a) maps the evolution of the ratio of surface roughness change of LBS5 with increasing normal load. The flattened *RMS* roughness, RMS_f, decreases gradually until the normal load reaches 60 N, most probably due to the flattening of the asperities from initial contact, after which it starts increasing. The onset of cracks accompanied by significant plastic deformation of the bulk at higher loads could be the cause of the roughening of the surface. For grain LBS2 (Fig. 11b), which did not fail, the value of RMS_f reduced until 40 N was reached, after which it increased almost linearly with increasing normal load. While significant bulk plastic deformation would have flattened the curvature of the surface at the contact, by using the motif extraction method, the effect of the surface curvature on the calculation of RMS_f had been removed (Boulanger, 1992). The increase of surface roughness might therefore be the result of surface damage caused by the plastic deformation of the bulk at the higher normal loads. Different from LBS2 and LBS5, the surface roughness of LBS26, for which the contact behaviour is mainly elastic, continues decreasing with increasing normal loading, despite plastic deformation of the bulk occurring at the load of 80 N (Fig. 11c).

The overall response of the 30-grain sample is represented next, using Weibull cumulative distribution function (Eq. 2) to represent the roughness and map its change during loading. Figure 12 shows the cumulative distributions of RMS_f at different load levels for the

30-grain sample tested, although for clarity in the figure only ten evenly distributed data for each load level are presented. The data for loads higher than 100 N is omitted as at these very high loads damage of the bulk caused less consistent changes in roughness in the different grains. The curves in Fig. 12 were fitted by the wblfit function of MATLAB, specific to the Weibull distribution. A good agreement was achieved by using the values λ=436.8 μm and k=5.48 at the load of 10 N (Fig. 13). From Table 2, which summarises the values of the two statistical parameters for the different load levels with the coefficients of determination (R^2), it can be concluded that the Weibull function fits all the experimental data, even those obtained after compression and therefore after change to the surface texture, but before significant damage to the particle.

The distribution curve describing the roughness of the grains gradually shifts leftwards with increasing normal load (Fig. 12), suggesting that both parameters λ and k are load dependent, although the change in scale seems more significant than the change in shape of the curve. The values of the two parameters are plotted against the normal load in Fig. 14. The scale parameter λ decreases fast until the normal load reaches 10 N, from a value of 0.462 μm to 0.437 μm, then the rate of reduction decreases. This reflects the plastic deformation of the surface asperities from initial contact, which had for effect to smoothen the surface even at low load levels. The slower reduction in surface roughness with further compression could be due to a gradual increase of the area at the existing contact points rather than an increase in the number of contact points being flattened. The real contact area was not determined so it is not possible to state whether the relationship between the load and the plastic contact area is linear (i.e. obeys the friction law) or non-linear. The bulk plastic deformation occurring at the higher loads may also be a factor for the slowing down of the reduction in surface roughness. The shape parameter k increases slightly with increasing load, indicating that the distribution of surface roughness of the thirty LBS grains becomes more uniform, the random processes creating the natural surfaces during their geological history gradually erased by the compression.

Conclusions

A series of single particle compression tests were carried out on LBS grains by a custom-made loading apparatus and the surface roughness at the contact points of the grains with the rigid loading platen was measured after each compression test by an optical interferometer. The evolution of surface roughness and the plastic deformation of each sand grain under compression was investigated based on the three-dimensional images and the two-dimensional profiles of the surfaces, respectively.

It was found that the asperities on the surface of the sand grains deformed plastically at the initial contact and the number of asperities flattened increased with increasing normal load. With increasing load, the possibility of the bulk deforming plastically increases. Through the comparison of the profiles of the surfaces at different levels of normal load, three stages of plastic deformation of the grains under compression could be identified: asperities plastic deformation domain, asperities and contact bulk plastic deformation, and contact bulk plastic deformation domain.

The main factor in differences between contact behaviour of individual sand grains was found to be the curvature of the surface in contact with the loading platen, the higher the surface curvature the smaller the contact area between the sand grains and the loading platen and therefore the easier for the sand grains with higher surface curvature to experience bulk plastic deformation.

During the asperity plastic deformation regime, the modified Hertz theory which takes surface roughness into consideration could better predict the load-displacement relationship of LBS grains under normal loading than the classical Hertz theory. However, due to the occurrence of the significant plastic deformation of the bulk at the contact, neither Hertz theory nor the modified Hertz theory was found to be applicable at higher loads. An elasto-plastic contact model which could take the plastic deformation of the bulk into consideration is needed for the DEM simulation of sand.

The evolution of surface roughness of individual sand grains with increasing normal load was found to vary with each other. The flattening of the asperities at the initial contact could reduce the surface roughness while the plastic deformation of the bulk could both smoothen and roughen the surfaces. Analysis of the sample of 30 tested sand grains, using cumulative distributions of the flattened roughness RMS_f, at the different load levels, showed that they were fitted by the Weibull function, even under compression, and that the two statistical parameters of the function are normal load dependent until significant bulk deformation occurs. At small loads, less than 10 N, which corresponds to the inter-particle forces for common engineering cases, the surface roughness of the sand grains decreases with increasing normal load, rapidly reaching a constant roughness.

Acknowledgements

The authors gratefully acknowledge Vincenzo Nardelli and Matthew Coop for their great help with designing and setting up the compression tests. Thank you also to Hongwei Yang for his support throughout this project. This research was funded by the Research Council of Hong Kong, award TR22-603-15N.

Appendix A Contact between two smooth spheres: Hertz' model

When two smooth spheres are pressed against each other by a normal force P, a small hemispherical contact area is created, with a circular boundary of radius a. From Hertz' theory (1882), the mutual approach δ_N between the two spheres is estimated from:

$$\delta_N = \left(\frac{9P^2}{16RE_*^2} \right)^{1/3} = \frac{a^2}{R} \tag{a.1}$$

where $1/R=1/R_1+1/R_2$, and $1/E_*=(1-\nu_1^2)/E_1+(1-\nu_2^2)/E_2$, the subscripts indicating the two bodies in contact; R_i is the radius of sphere i, E_i and ν_i are Young's modulus and Poisson's ratio of sphere i, respectively. The radius of the contact area can be calculated from:

$$a = \left(\frac{3PR}{4E*} \right)^{1/3} \tag{a.2}$$

In the case of contact between a smooth sphere and a smooth flat half surface, the effective radius R is simply equal to the sphere radius.

Appendix B Contact between two rough spheres: modified Hertz' model

The surface roughness is quantified by the root-mean-square of the heights to the mean plane of the surface (Thomas, 1982):

$$RMS = \sqrt{\frac{1}{M}\frac{1}{N}\sum_{i=1}^{M}\sum_{j=1}^{N}\left(Z(i,j)^2 \right)} \tag{b.1}$$

where M and N are the number of points along the X and Y directions respectively, and Z(i,j) is the height of a point to the mean plane of the surface. Greenwood *et al*. (1984) and Johnson (1985) proposed to quantify roughness by a non-dimensional parameter α:

$$\alpha = \frac{RMS^* R}{a^2} \tag{b.2}$$

where RMS^* is the combined surface roughness, calculated from $RMS^{*2}=RMS_{f1}^2+RMS_{f2}^2$, RMS_{fi}: the flattened root-mean-square roughness of sphere i. One of the effects of roughness is to increase the apparent nominal contact area (e.g. Greenwood & Williamson, 1966), so denoting a^{smooth} the radius calculated from (Eq. a.2, in Appendix A) for smooth spheres, Yimsiri & Soga (2000) proposed that the ratio between the radius of the rough contact area, a^{rough}, to a^{smooth} is a function of α, the expression below derived from experimental data on hard steel ball against hard steel flat reported in Greenwood *et al*. (1984):

$$a^{rough} = (\frac{-2.8}{\alpha+2} + 2.4)a^{smooth} \tag{b.3}$$

By implementing the contact radius for rough spheres into Hertz's equations, we obtain a load-displacement relationship for rough surfaces, which we call modified Hertz' model:

$$\delta^{rough} = \frac{1}{R}\left[(\frac{-2.8}{\alpha+2} + 2.4)a^{smooth}\right]^2 \tag{b.4}$$

References

Altuhafi, F. N. & Coop, M. R. (2011). Changes to particle characteristics associated with the compression of sands. *Géotechnique* **61**, No. 6, 459-471, https://doi.org/10.1680/geot.9.P.114.

Archard, J. F. (1957). Elastic deformation and the law of friction. *Proceedings of the Royal Society A* **243**, No. 1233, 190-205.

Bahrami, M., Yovanovich, M. M. & Culham, J. R. (2004). *A compact model for spherical rough contacts*. International Joint Tribology Conference, American Society of Mechanical Engineers, 1147-1156.

Barreto Gonzalez, D. (2009) *Numerical and experimental investigation into the behaviour of granular materials under generalised stress states*. PhD thesis, University of London, UK.

Boulanger, J. (1992). The "Motif" method: An interesting complement to ISO parameters for some functional problems. *International Journal of Machine Tools and Manufacture* **32**, No. 1-2, 203-209.

Brzesowsky, R. H., Spiers, C. J., Peach, C. J. & Hangx, S. J. T. (2011). Failure behaviour of single sand grains: theory versus experiment. *Journal of Geophysical Research* **116**, No. B6.

Cavarretta, I., Coop, M. R. & O'Sullivan, C. (2010). The influence of particle characteristics on the behaviour of coarse-grained soils. *Géotechnique* **60**, No. 6, 413-423, https://doi.org/10.1680/-geot.2010.60.6.413.

Cavarretta, I., O'Sullivan, C., Ibraim, E., Lings, M., Hamlin, S., & Wood, D. M. (2012). Characterization of artificial spherical particles for DEM validation studies. *Particuology* **10**, No. 2, 209-220.

Cavarretta, I., O’Sullivan, C. & Coop, M. R. (2017). The relevance of roundness to the crushing strength of granular materials. *Géotechnique* **67**, No. 4, 301-312, https://doi.org/10.1680/jgeot.15.P.226.

Chang, W. R., Etsion, I. & Bogy, D. B. (1987). An elastic-plastic model for the contact of rough surfaces. *Journal of tribology* **109**, No. 2, 257-263.

Cooper, M. G., Mikic, B. B. & Yovanovich, M. M. (1969). Thermal contact conductance. *International Journal of Heat and Mass Transfer* **12**, 279-300.

Fogale (2005). *Fogale nanotech user manual version* 1.5. Nimes, France: Fogale.

Greenwood, J. A. & Williamson, J. P. (1966). Contact of nominally flat surfaces. *Proc. R. Soc. Lond. A* **295**, No. 1442, 300-319.

Greenwood, J. A. & Tripp, J. H. (1967). The elastic contact of rough spheres. *Journal of Applied Mechanics* **34**, No. 1, 153-159.

Greenwood, J. A., Johnson, K. L. & Matsubara, E. (1984). A surface roughness parameter in Hertz contact. *Wear* **100**, No. 1-3, 47-57.

Greenwood, J. A. & Wu, J. J. (2001). Surface Roughness and Contact: An Apology. *Meccanica* **36,** 617–630.

Hanaor, D. A. H., Gan, Y. & Einav, I. (2013). Effects of surface structure deformation on static friction at fractal interfaces. *Géotechnique Letters* **3**, No. 2, 52-58.

Hertz, H. (1882). Über die Berührung fester elastischer Körper. *J. reine und angewandte Mathematik* **92**, 156-171 (in German).

Holm, R. (1938). The friction force over the real area of contact. *Wiss. Veroff. Siemens-Werk* **17**, No. 4, 38-42.

Johnson, K.L. (1985). *Contact Mechanics*. Cambridge, UK: Cambridge University Press.

Jaeger, J. C., Cook, N. G. & Zimmerman, R. (2007). *Fundamentals of rock mechanics,* 4 edn. Oxford, UK: Wiley-Blackwell.

Jamari, J. & Schipper, D. J. (2007). Deformation due to contact between a rough surface and a smooth ball. *Wear* **262**, No. 1-2, 138-145.

Kogut, L. & Etsion, I. (2003). A finite element based elastic-plastic model for the contact of rough surfaces. *Tribology transactions* **46**, No. 3, 383-390.

Li, L., Etsion, I. & Talke, F.E. (2010) Elastic-plastic spherical contact modelling including roughness effects. *Tribol. Lett.* **40**, 357-363.

Mavko, G., Mukerji, T. & Dvorkin, J. (1998). *The rock physics handbook, second edition: tools for seismic analysis of porous media*. Cambridge, UK: Cambridge University Press.

Nadimi, S., Fonseca, J., Andò, E. & Viggiani, G. (2020). A micro finite-element model for soil behaviour: experimental evaluation for sand under triaxial compression. *Géotechnique* **70**, No. 10, 931-936, https://doi.org/10.1680/jgeot.18.T.030.

Nardelli, V. (2017). *An experimental investigation of the micromechanical contact behaviour of soils*. PhD thesis, City University of Hong Kong, Hong Kong, P. R. China.

Nardelli, V., Coop., M. R., Andrade, J. E. & Piccagnella, F. (2017). An experimental investigation of the micromechanics of Eglin sand. Powder Technology 312, 166-174.

Nardelli, V. & Coop, M. R. (2019). The experimental contact behaviour of natural sands: normal and tangential loading. *Géotechnique* **69**, No. 8, 672-686, https://doi.org/10.1680/jgeot.17.P.167.

Otsubo, M., O'Sullivan, C. & Sim, W. W. (2014). *A methodology for accurate roughness measurements of soils using optical interferometry*. Geomechanics from Micro to Macro, London, UK, 1117-1122.

Otsubo, M., O'Sullivan, C., Sim, W. W. & Ibraim, E. (2015). Quantitative assessment of the influence of surface roughness on soil stiffness. *Géotechnique* **65**, No. 8, 694-700, https://doi.org/-10.1680/geot.14.T.028.

Persson, B. N. J. (2001). Elastoplastic contact between randomly rough surfaces. *Physical Review Letters* **87**, No. 11, 116101-1.

Santamarina, C. & Cascante, G. (1998). Effect of surface roughness on wave propagation parameters. *Géotechnique* **48**, No. 1, 129-136, https://doi.org/10.1680/geot.1998.48.1.129.

Senetakis, K., Coop, M. R. & Todisco, M. C. (2013). The inter-particle coefficient of friction at the contacts of Leighton Buzzard sand quartz minerals. *Soils and Foundations* **53**, No. 5, 746-755.

Sandeep, C. S. & Senetakis, K. (2018a). Grain-scale mechanics of quartz sand under normal and tangential loading. *Tribology International* **117**, 261-271.

Sandeep, C. S. & Senetakis, K. (2018b). Effect of Young's modulus and surface roughness on the inter-particle friction of granular materials. *Materials* **11**, No. 2, 217.

Tabor, D. (1951). The hardness and strength of metals. *J. Inst. Met* **79**, 1-18.

Thomas, T. R. (1982). *Rough surfaces*. London, UK: Longman.

Wadell, H. (1932). Volume, shape, and roundness of rock particles. *The Journal of Geology* **40**, No. 5, 443-451.

Wang, W. & Coop, M. R. (2016). An investigation of breakage behaviour of single sand particles using a high-speed microscope camera. *Géotechnique* **66**, No. 12, 984-998, https://doi.org/10.1680/jgeot.15.P.247.

Wang, W. (2017). *An investigation of breakage behaviour and micro-mechanics of sand particles using digital imaging techniques*. PhD thesis, City University of Hong Kong, Hong Kong, P. R. China.

Weber, B., Suhina, T. Junge, T., Pastewka, L., Brouwer, A. M. & Bonn, D. (2018). Molecular probes reveal deviations from Amontons' law in multi-asperity frictional contacts. *Nature communications* **9**, 888.

Weibull, W. (1951). Wide applicability. *Journal of applied mechanics* **103**, No. 730, 293-297.

Yang, H., Baudet, B. A. & Yao, T. (2016). Characterization of the surface roughness of sand particles using an advanced fractal approach. *Proceedings of the Royal Society A* **472**, 2194, 20160524.

Yao, T., Baudet, B. A. & Lourenço, S. D. (2018). Quantification of the surface roughness of quartz sand using optical interferometry. *Meccanica* **54**, 741-748.

Yao, T. (2019). *Characterization of soil grain surface roughness and its change with normal loading.* PhD thesis, The University of Hong Kong, Hong Kong, P. R. China.

Yimsiri, S. & Soga, K. (2000). Micromechanics-based stress-strain behaviour of soils at small strains. *Géotechnique* **50**, No. 5, 559-571, https://doi.org/10.1680/geot.2000.50.5.559.

Zhao, B., Wang, J., Coop, M. R., Viggiani, G. & Jiang, M. (2015). An investigation of single sand particle fracture using X-ray micro-tomography. *Géotechnique* **65**, No. 8, 625-641, https://doi.org/10.1680/geot.4.P.157.

Table 1. Summary of the physical properties of Leighton Buzzard sand

Parameters	Values	References
d_{mean} (mm)	2.65	
RMS_f (nm)	416±65	
E (GPa)	94-98	Mavko et al., 1998
G (GPa)	44-46	Jaeger et al., 2007
v	0.065-0.068	
H (GPa)	6.2	Wang, 2017

Table 2. Summary of the two parameters of the Weibull distribution of RMS_f of 30 tested LBS under different normal loads

Force/N	0	2	5	10	20	40	80
λ/nm	461.53	444.39	440.18	436.79	433.73	430.14	419.75
k	5.64	5.49	5.53	5.48	5.55	5.59	5.85
R^2	0.994	0.992	0.994	0.991	0.992	0.993	0.991

(a)

(b)

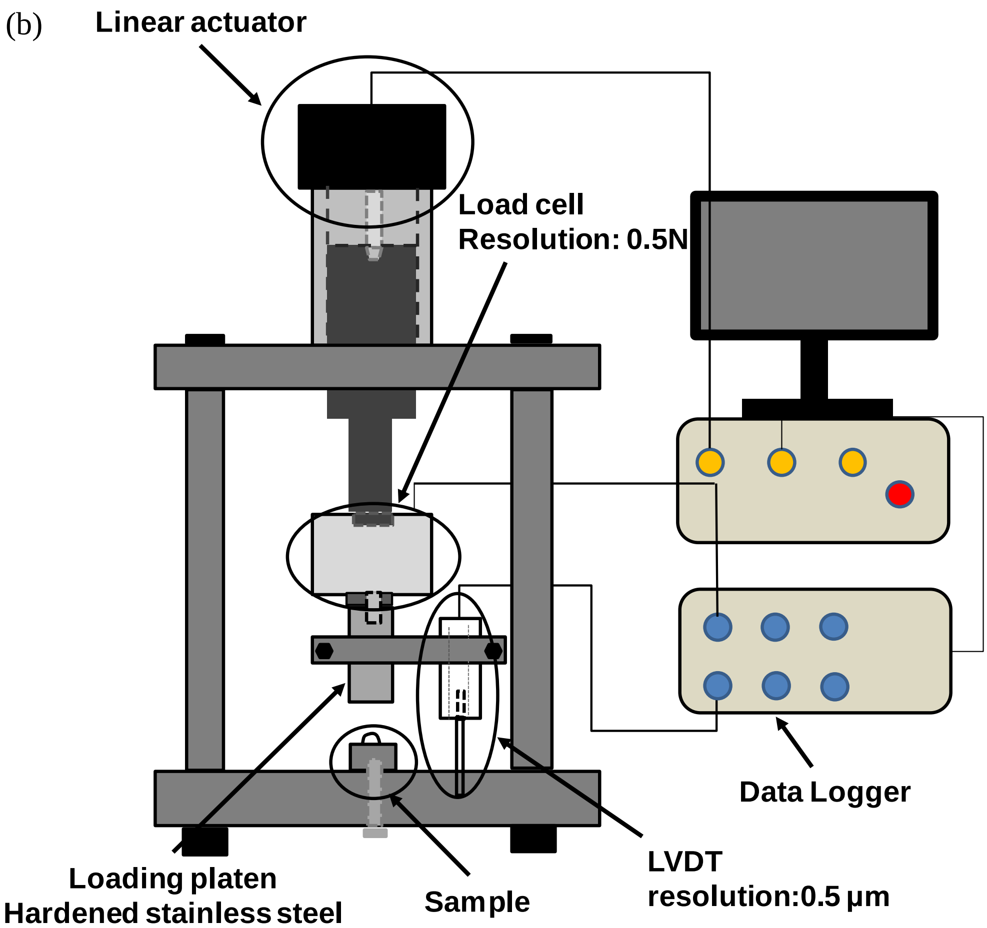

Fig. 1. (a) Image of the Leighton Buzzard sand grains with particle size of 2.36-5 mm; (b) Schematic diagram of the custom-made single particle loading apparatus

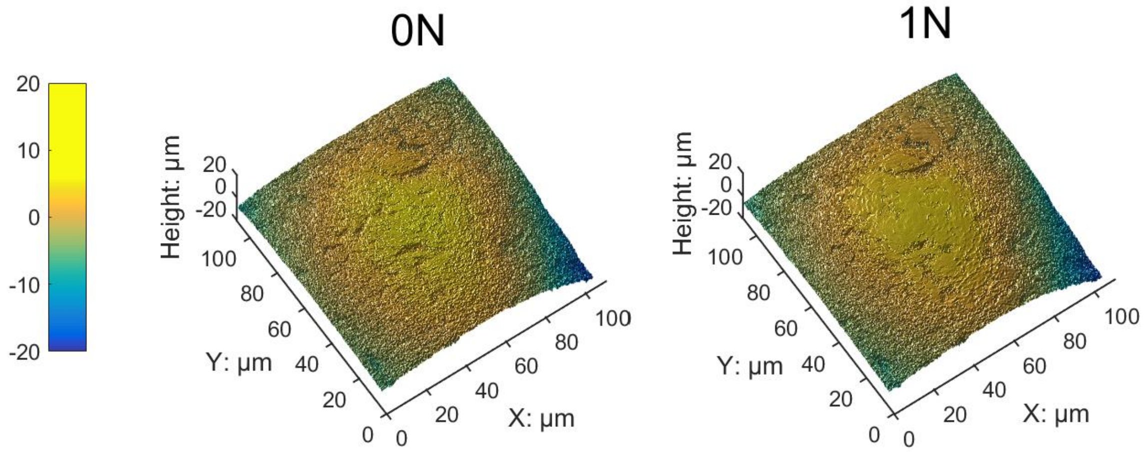

Fig. 2. Surfaces of LBS5 before and after compression to 1 N

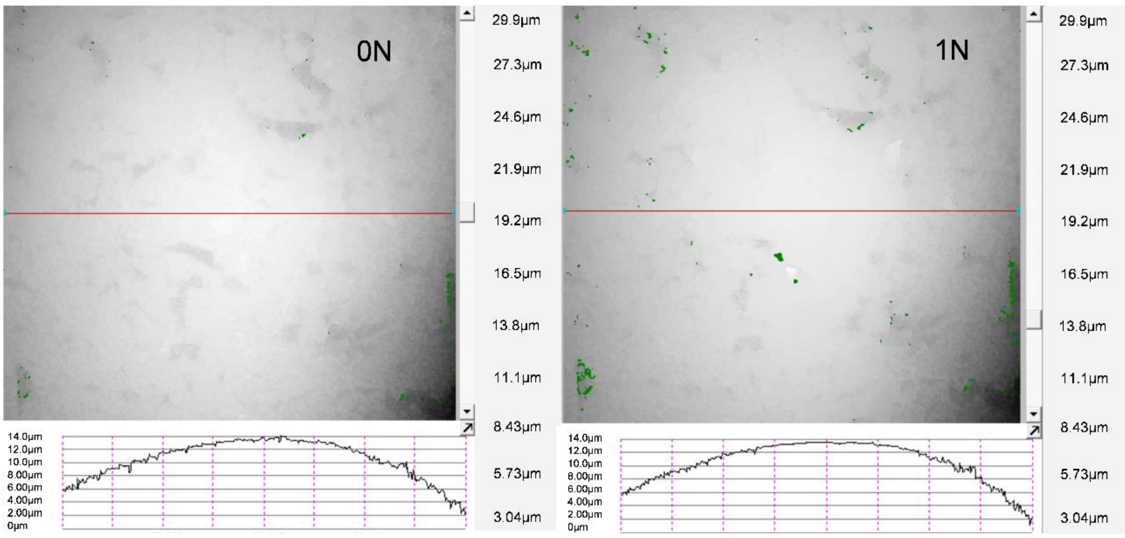

Fig. 3. Two-dimensional image of the surfaces of LBS5 with profiles of the centre-line along Y direction before and after compression to 1 N

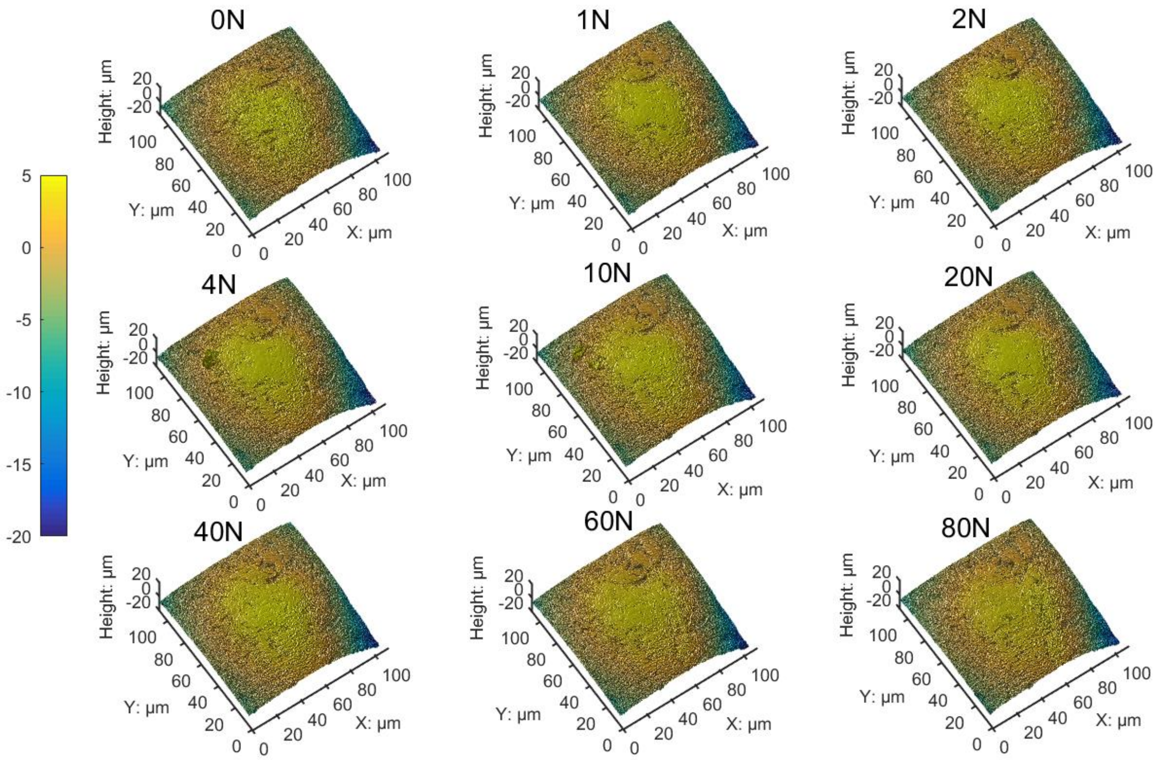

Fig. 4. Surfaces in contact with the loading platen of LBS5 at different load levels

(a)

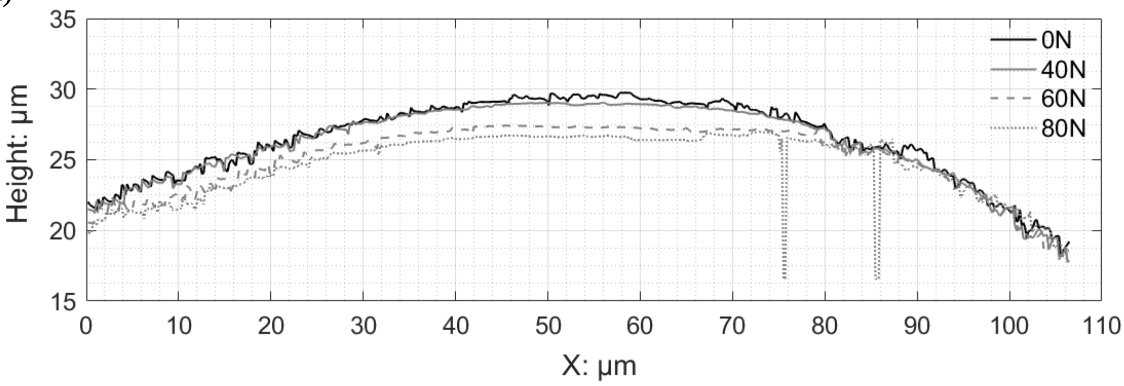

(b)

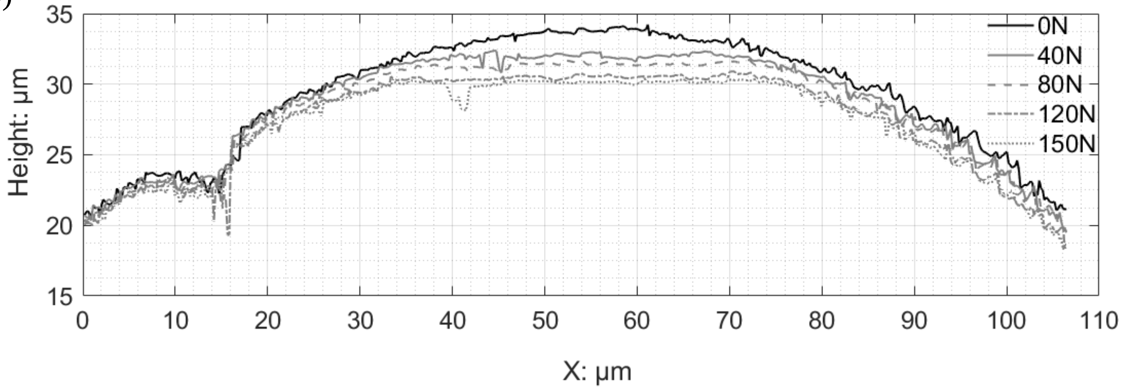

(c)

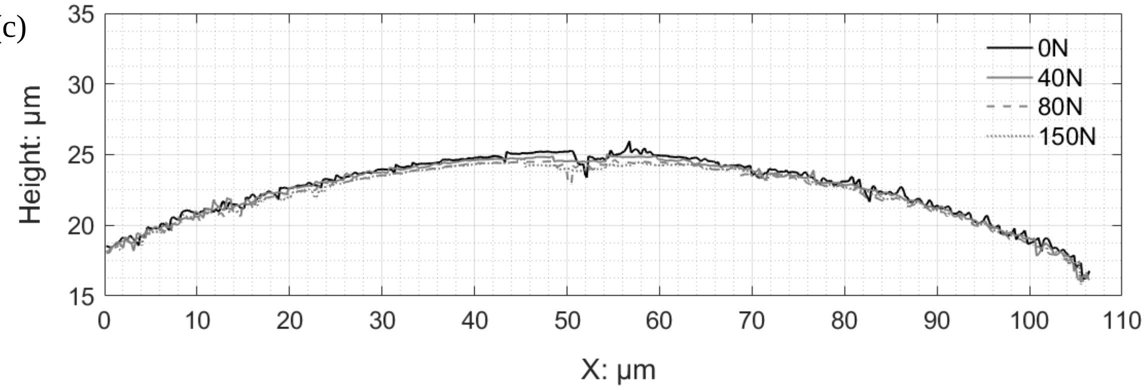

Fig. 5. Matching results of the profiles of the centre-lines of the surfaces in contact with the loading platen at different loads: (a) LBS5; (b) LBS2; (c) LBS26

(a)

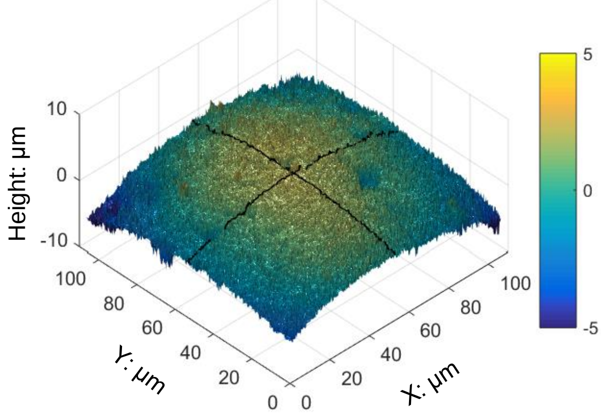

(b)

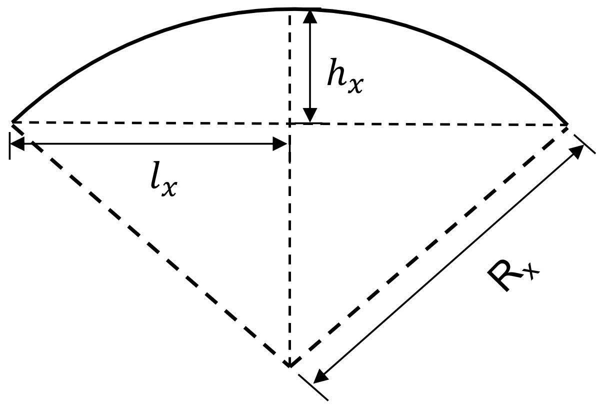

Fig. 6. The illustration of the estimation of the radius of the curvature of the surface in contact: (a) The outlines used to calculate the curvature at X, Y directions; (b) Illustration of the simplified method to calculate radius of the curvature at X direction

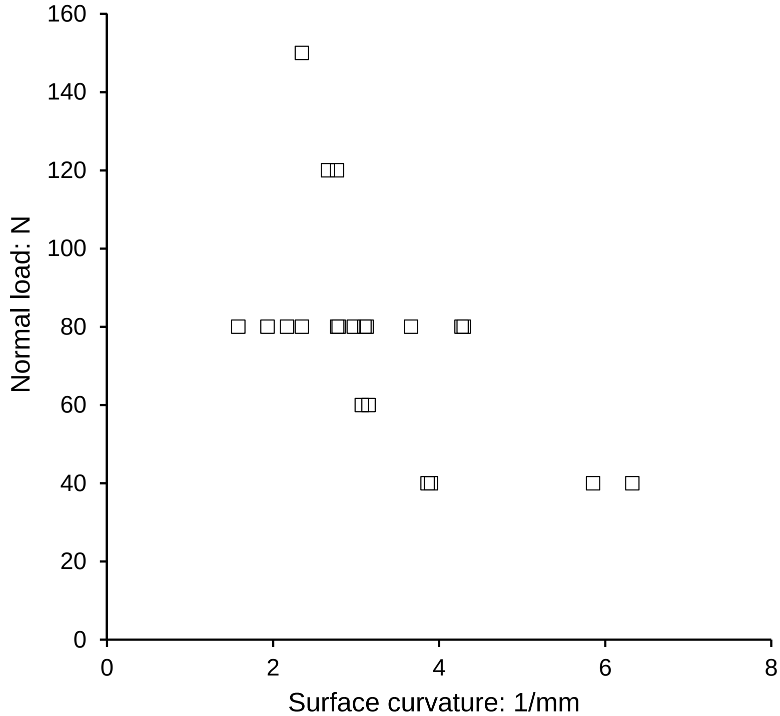

Fig. 7. The effect of surface curvature ($1/R_c$) on the occurrence of bulk plastic deformation of the sand grains

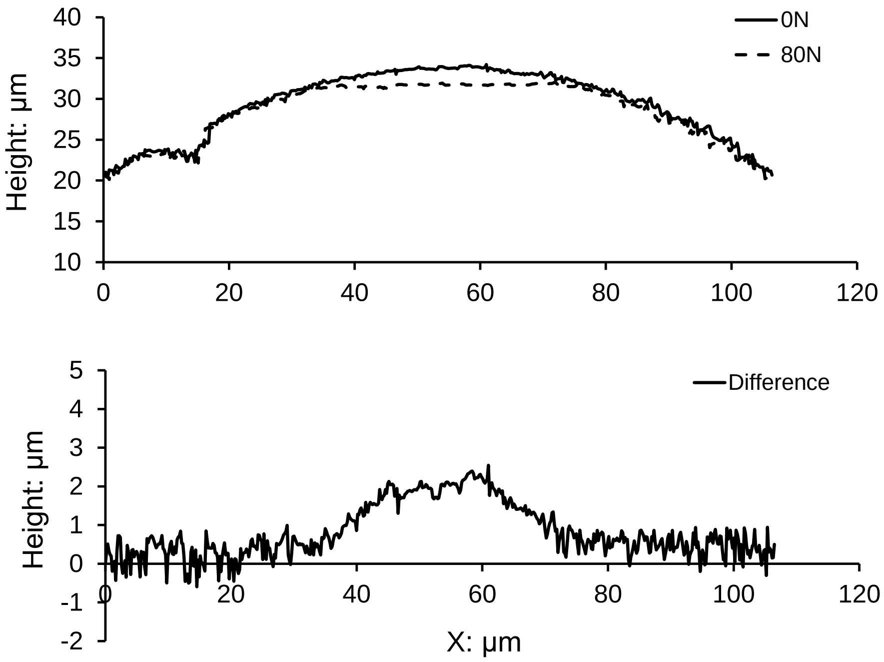

Fig. 8. An example of quantifying the plastic deformation of the LBS grain under compression

(a)

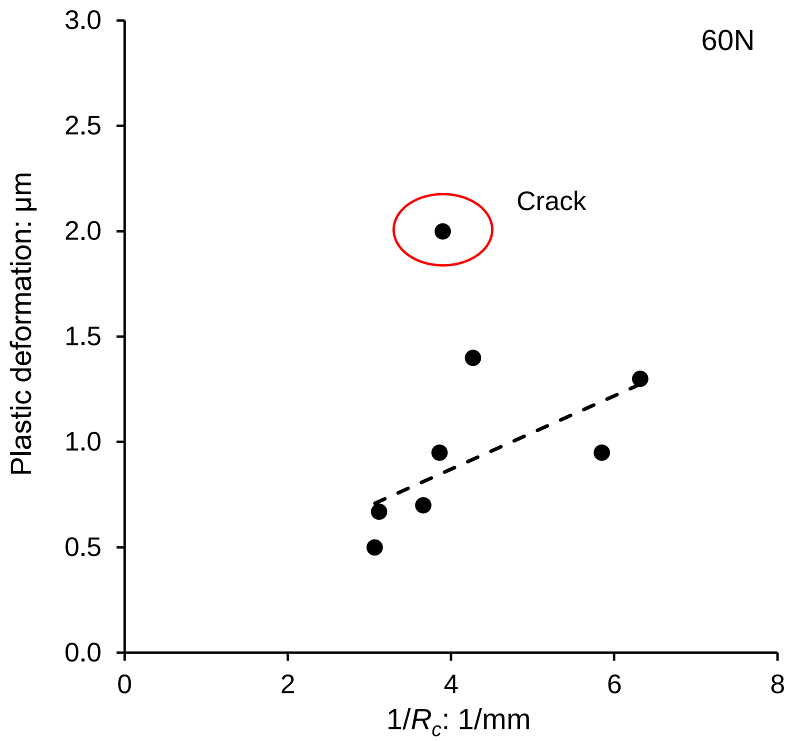

(b)

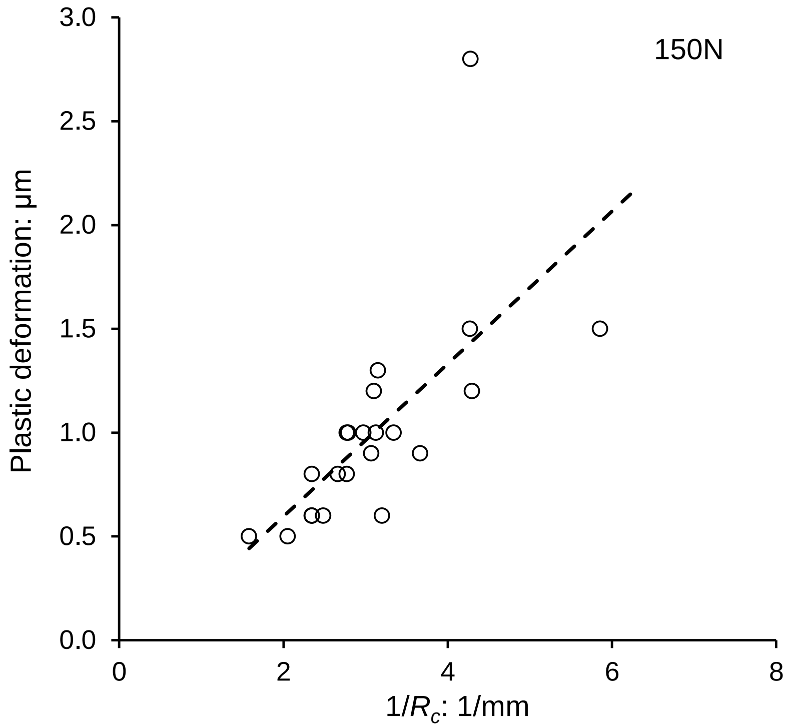

Fig. 9. Relationship between the plastic deformation of the LBS grains and the surface curvature ($1/R_c$): (a) at the load of 60 N; (b) at the load of 150 N

(a)

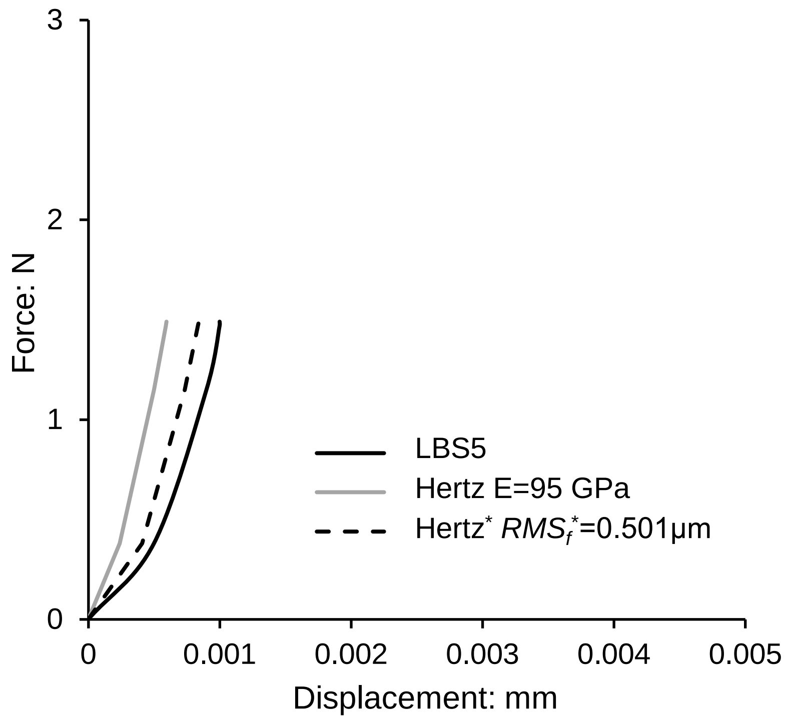

(b)

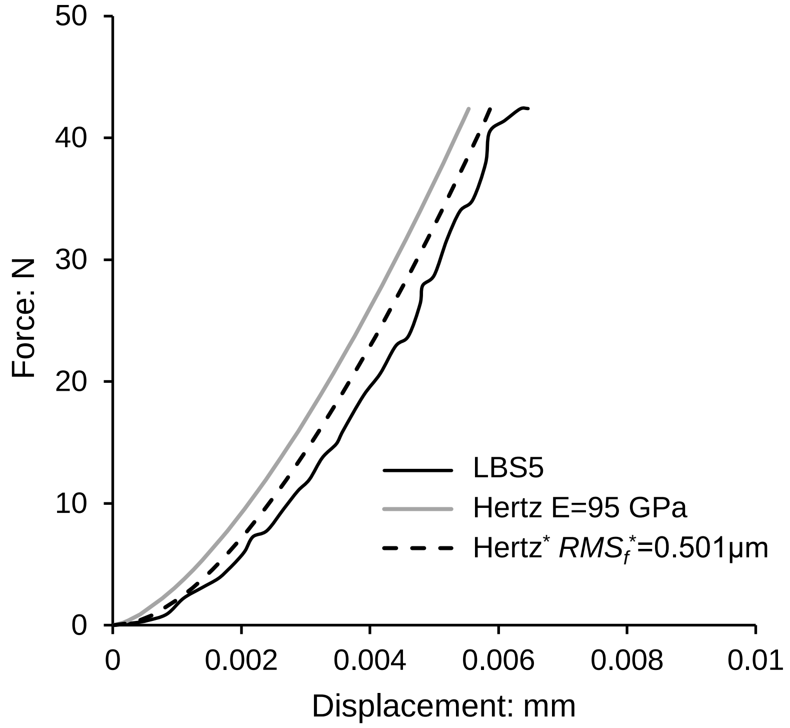

Force: N
Displacement: mm
0
10
20
30
40
50
0
0.002
0.004
0.006
0.008
0.01
LBS5
Hertz E=95 GPa
Hertz* RMS_f^*=0.501μm

(c)

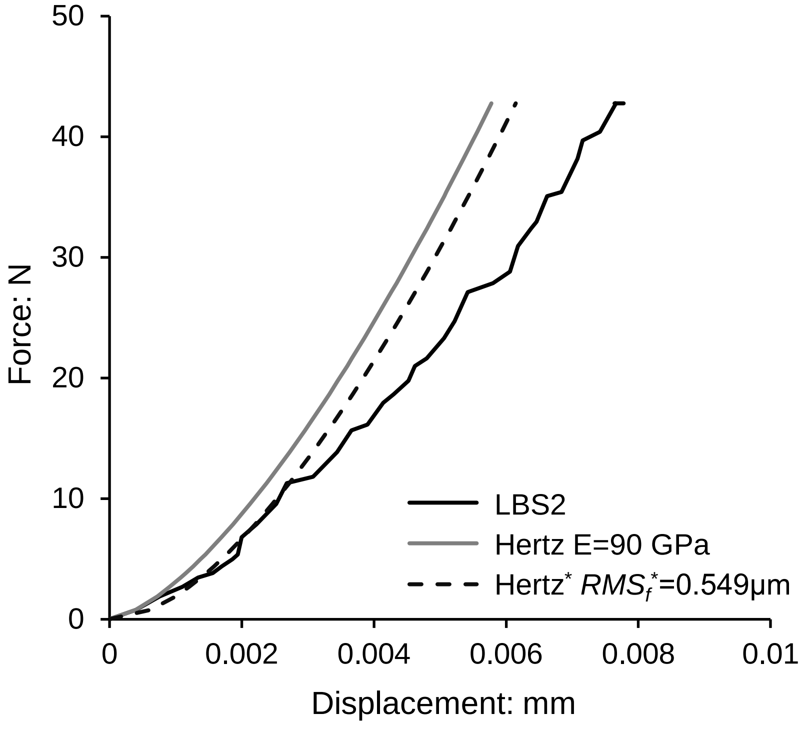

Force: N
Displacement: mm
0
10
20
30
40
50
0
0.002
0.004
0.006
0.008
0.01
LBS2
Hertz E=90 GPa
Hertz* RMS_f^*=0.549μm

(d)

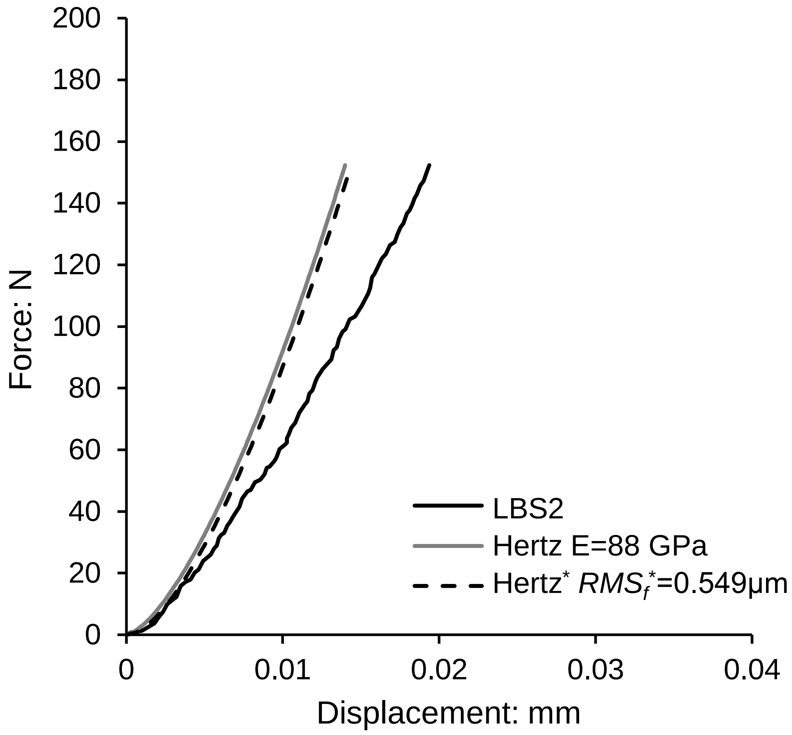

200
180
160
140
120
100
80
60
40
20
0
Force: N
0
0.01
0.02
0.03
0.04
Displacement: mm
LBS2
Hertz E=88 GPa
Hertz* RMSf*=0.549μm

(e)

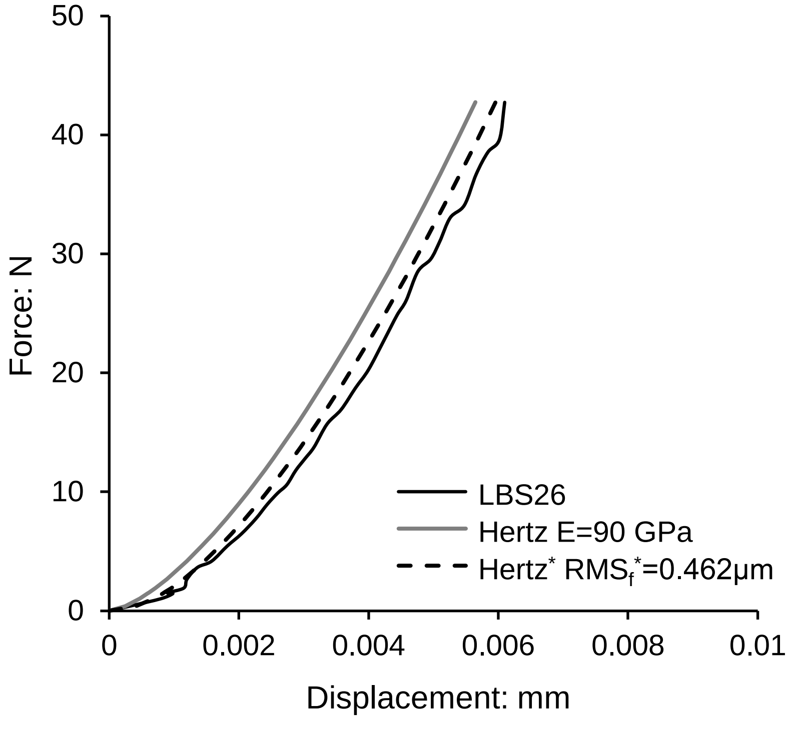

50
40
30
20
10
0
Force: N
0
0.002
0.004
0.006
0.008
0.01
Displacement: mm
LBS26
Hertz E=90 GPa
Hertz* RMSf*=0.462μm

(f)

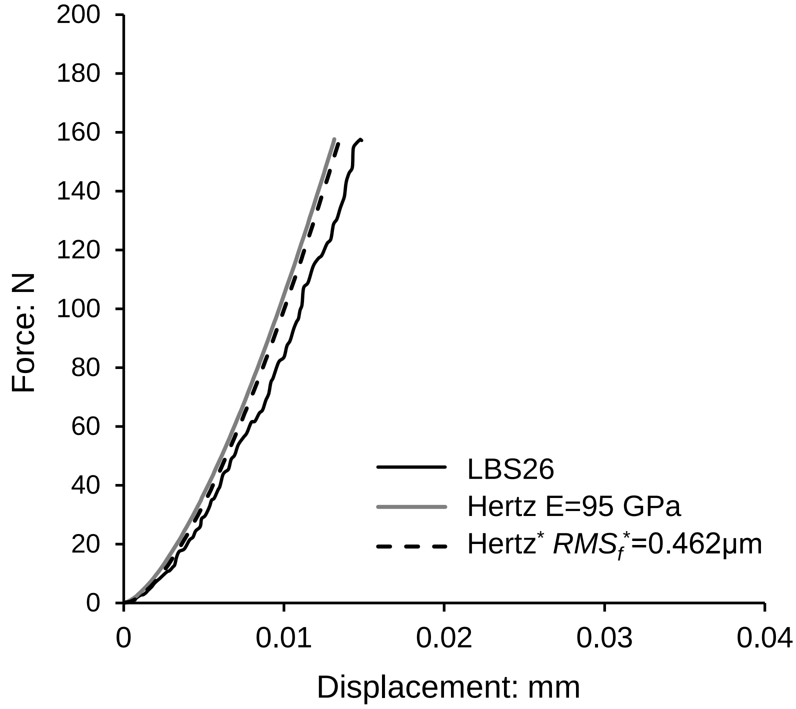

Fig. 10. Comparisons between the load-displacement curves and predictions of Hertz theory and modified Hertz theory: (a) LBS5 at the load of 1 N; (b) LBS5 at the load of 40 N; (c) LBS2 at the load of 40 N; (d) LBS2 at the load of 150 N; (e) LBS26 at the load of 40 N; (f) LBS26 at the load of 150 N

(a)

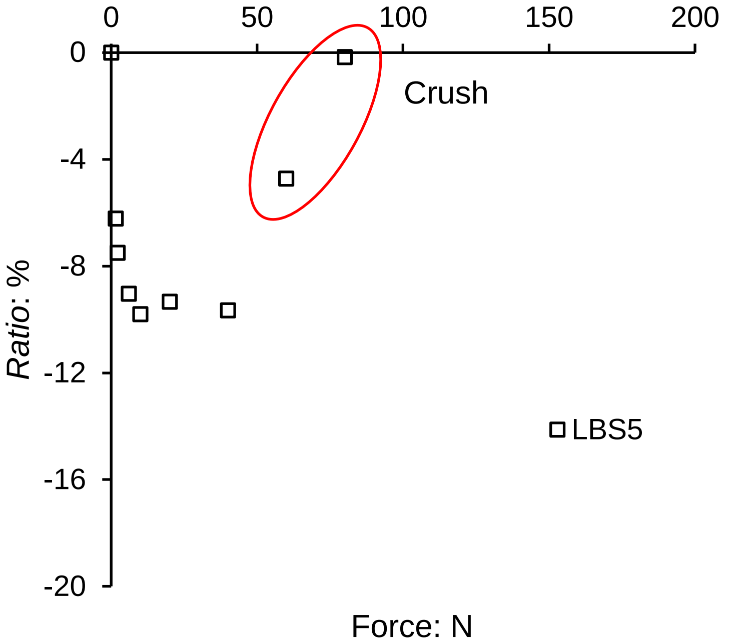

(b)

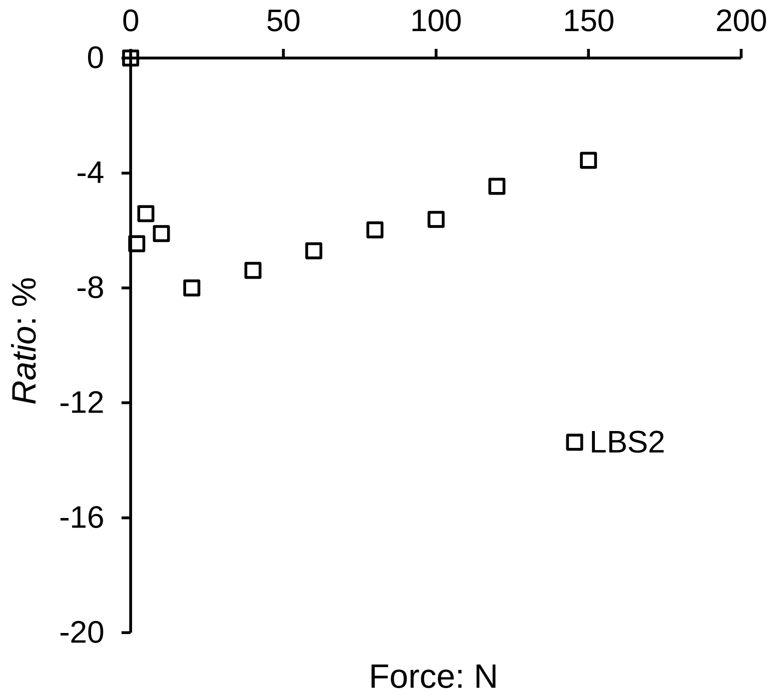

(c)

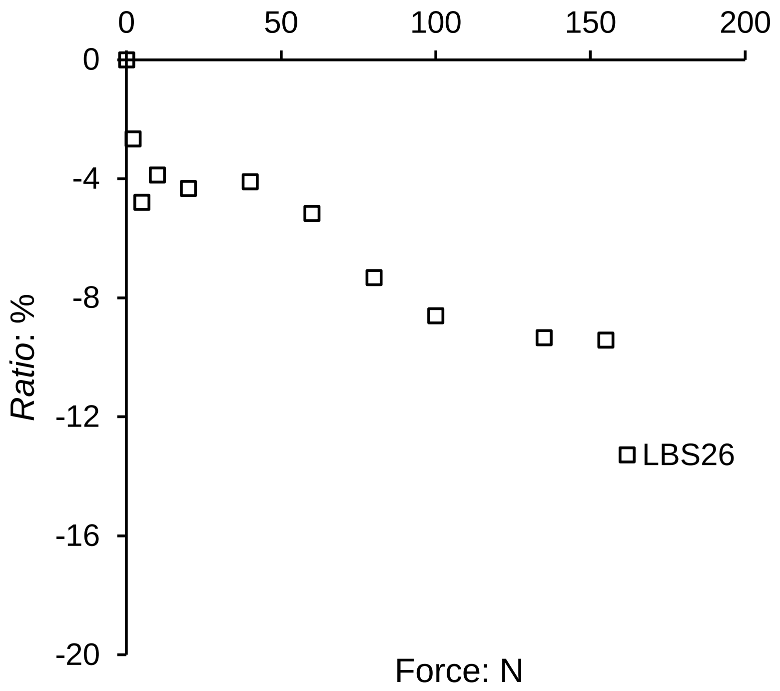

Fig. 11. Relationship between the normal load and the *Ratio* of change in surface roughness of individual sand grains: (a) LBS5; (b) LBS2; (c) LBS26

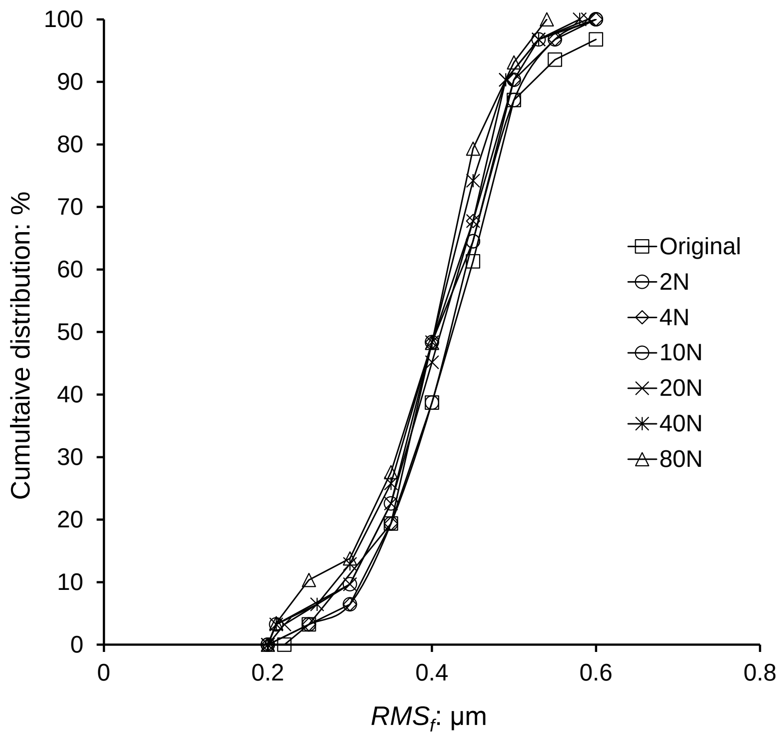

Fig. 12. Evolution of the cumulative distributions of RMS_f of the tested LBS grains with increasing normal load

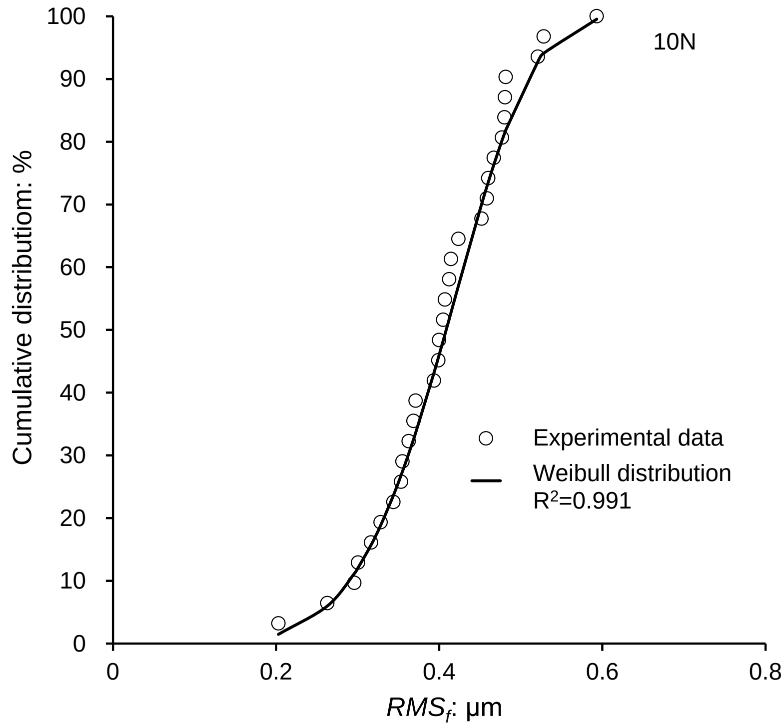

Fig. 13. Weibull function fitting of the cumulative distribution of RMS_f of thirty LBS grains when the normal load is 10 N

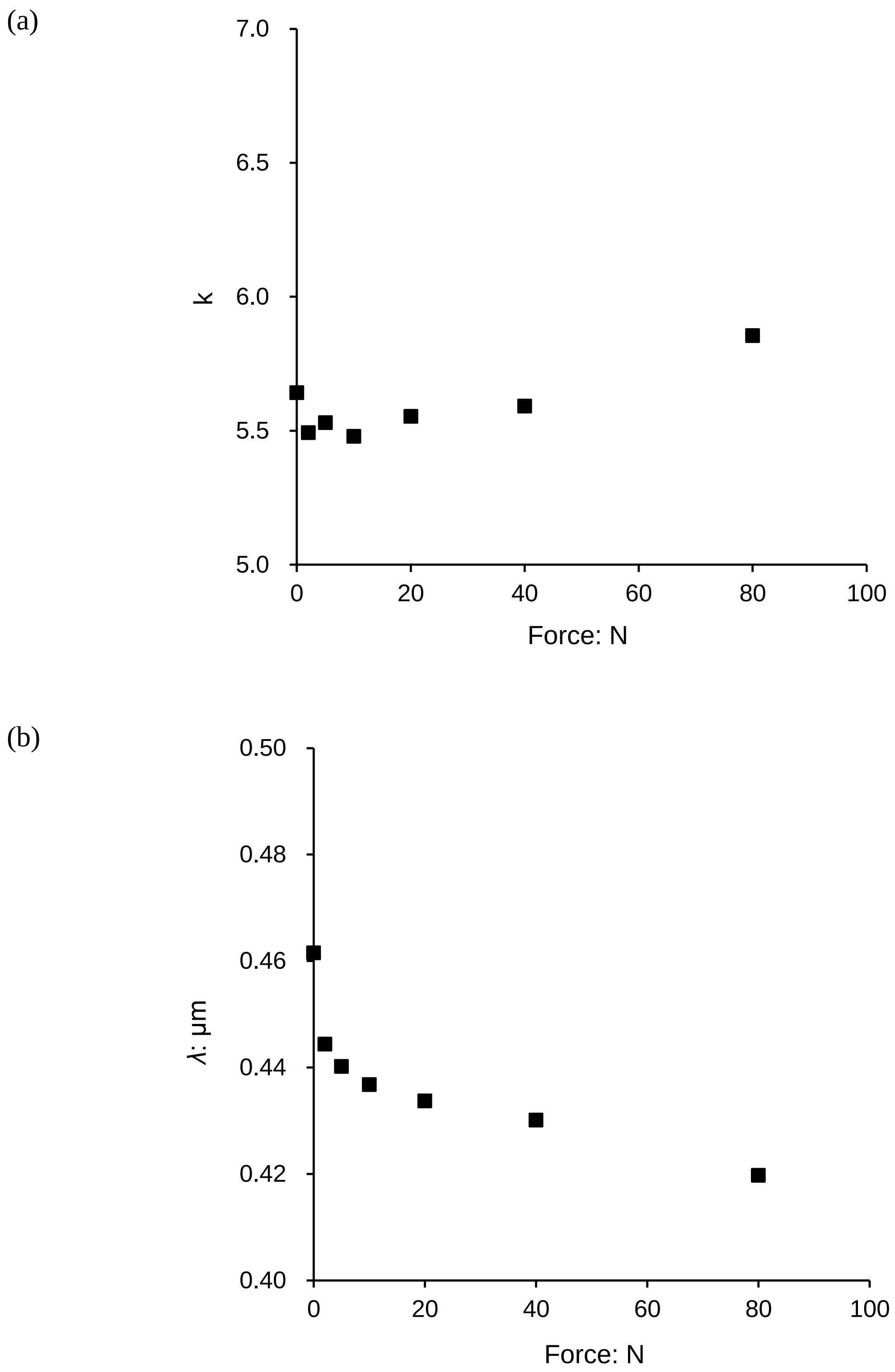

Fig. 14. Relationship between the two statistical parameters of Weibull function and normal loads: (a) P-λ; (b) P-k